Morphogenesis of the islets of Langerhans is guided by extra-endocrine Slit2/3 signals

Jennifer M. Gilbert[1], Melissa T. Adams[1], Nadav Sharon[2], Hariharan Jayaraaman[1], Barak Blum[1*]

[1]Department of Cell and Regenerative Biology, University of Wisconsin-Madison School of Medicine and Public Health, 1111 Highland Avenue, Madison, WI 53705, USA.

[2]Department of Stem Cell and Regenerative Biology, Harvard University, 7 Divinity Avenue, Cambridge, MA, 02138, USA.

*Corresponding author: Barak Blum; bblum4@wisc.edu

Abstract

The spatial architecture of the islets of Langerhans is vitally important for their correct function, and alterations in islet morphogenesis often result in diabetes mellitus. We have previously reported that function of Roundabout (Robo) receptors, selectively in β-cells, is required for proper islet morphogenesis. As part of the Slit-Robo signaling pathway, Robo receptors work in conjunction with Slit ligands to mediate axon guidance, cell migration, and cell positioning in development. However, the role of Slit ligands in islet morphogenesis has not yet been determined. Here we report that Slit ligands are expressed in overlapping and distinct patterns in both endocrine and non-endocrine tissues in late pancreas development. We show that function of either Slit2 or Slit3, which are predominantly expressed in the pancreatic mesenchyme, is required and sufficient for islet morphogenesis, while Slit1, which is predominantly expressed in the endocrine compartment, is dispensable for islet morphogenesis. We further provide evidence to suggest that Slit-Robo signaling in the pancreas influences endocrine cell-cell adhesion, not cell migration, during islet morphogenesis. These data add important understanding to the fundamental question of the formation of the unique architecture of the islets of Langerhans.

Introduction

Blood glucose homeostasis is regulated in the pancreas by clusters of endocrine cells called the islets of Langerhans. Islets consist of five different endocrine cell types (α, β, δ, PP, ε), which secrete glucagon, insulin, somatostatin, pancreatic polypeptide, and ghrelin, respectively. Murine islets exhibit a distinct cytoarchitecture consisting of a core of β-cells, surrounded by a mantle of α-, δ-, PP- and ε-cells. The β-cell core makes up roughly 80% of the islet mass, while the four other cell types make up the remaining 20% (Kim et al., 2009; Steiner et al., 2010). This cytoarchitecture is thought to be important for proper islet function, and loss of this architectural makeup is described in obesity and diabetes in both mice and humans (Baetens et al., 1978; Cabrera et al., 2006; Kilimnik et al., 2011; Roscioni et al., 2016). While the architectural features of islets have been well-documented, the mechanisms controlling this architecture are still largely unknown.

The Slit-Robo signaling pathway has roles in a number of developmental processes, primarily axon guidance, cell movement, and cell adhesion (Blockus and Chédotal, 2016; Chédotal, 2007; Wu et al., 2017; Ypsilanti and Chedotal, 2014; Ypsilanti et al., 2010). Slit ligand binding to Robo receptors can induce cell migration using repulsive or attractive cues in a context-dependent manner. In the developing mouse, Slit-Robo signaling provides a repulsive corridor to prevent migrating axons from straying from their path during innervation (Brose et al., 1999; Dickson and Gilestro, 2006). Slit-Robo binding inactivates Rho GTPases, inhibiting actin polymerization and driving the cell away from the direction of the Slit signal (Wu et al., 2017; Ypsilanti et al., 2010). Conversely, Slit uses attractive cues to promote vascular development and angiogenesis. In this context, Slit-Robo interactions activate Rho GTPases, inducing actin polymerization in the direction of the Slit signal (Rama et al., 2015; Wu et al.,

2017; Ypsilanti et al., 2010; Zhang et al., 2009). In both cases, Slit-Robo signaling activity is able to modulate cell-cell adhesion molecules, which aids cell migration (Tong et al., 2019; Wu et al., 2017). While Slit and Robo are a canonical signaling pair, both components have alternative binding partners; Slit ligands are able to bind semaphorins, ephrins, plexin, and neuronatin to regulate cell migration and metabolic function in specific tissues (Brose et al., 1999; Delloye-Bourgeois et al., 2015; Svensson et al., 2016; Wright et al., 2012). Robo receptors are capable of forming homodimers to induce axonal growth (Hivert, 2002).

We have recently described a role for Robo receptors in pancreatic islet architecture (Adams et al., 2018). Specifically, we showed that genetic deletion of *Robo1* and *Robo2* in β-cells (*Robo βKO*) results in loss of stereotypic murine islet architecture, without affecting β-cell differentiation or maturation. These Robo-depleted islets have a marked invasion of α- and δ-cells into the β-cell core. Additionally, *Robo βKO* islets have cell-cell adhesion defects. Given the conserved role of Slits as the canonical Robo ligands and our recent findings that Robo receptors regulate endocrine cell type sorting in the islet, we set to investigate the role of Slit ligands in islet morphogenesis.

Results

Slits ligands are expressed in different compartments in the developing mouse pancreas.

To test the hypothesis that Slits are involved in Robo-mediated control of islet architecture during development, we first examined whether any of the Slit ligands are expressed in the pancreas at the time of islet morphogenesis. We queried a gene expression database, generated by Krentz and colleagues (Krentz et al., 2018), which contains single-cell RNA-Seq data from embryonic mouse pancreata. We found that *Slit1* expression is present in a subset of endocrine progenitor cells at

embryonic day (E)15.5, and becomes enriched in β-cells by E18.5. *Slit2* and *Slit3* expression is distributed between pancreatic mesenchyme, acinar, and ductal cell types with negligible expression in the endocrine compartment at both time points (Figure 1).

To more precisely determine the localization of Slit ligands in the pancreas, we analyzed pancreata from $Slit1^{GFP}$, $Slit2^{GFP}$, and $Slit3^{LacZ}$ mice, which have knock-in reporters at their respective endogenous Slit loci (Plump et al., 2002; Yuan et al., 2003). We identified strong GFP expression in $Slit1^{GFP/+}$ mice both in E18.5 and adult islets. This staining pattern overlapped with insulin, indicating that *Slit1* is expressed in β-cells at both stages (Figure 2A). We were not able to detect $Slit2^{GFP}$ (Figure 2A) or $Slit3^{LacZ}$ (Figure 2B) in either the embryonic or the adult endocrine compartment. However, we detected both $Slit2^{GFP}$ and $Slit3^{LacZ}$ expression in tissues outside of the islet (Figure 2B and 2C). A previous report by Escot and colleagues identified *Slit3* expression in the mesenchyme (Escot et al., 2018). We concluded that *Slit1* is the predominant Slit ligand expressed inside the islets, and that *Slit2* and *Slit3* are expressed outside of the islet during pancreatic development.

Loss of a single Slit ligand does not compromise islet architecture.

Slit and Robo are conserved binding partners, and loss of Robo in the islets of *Robo βKO* mice results in severely altered islet architecture (Adams et al., 2018). We hypothesized that if Slits mediate Robo-regulated islet architecture, then eliminating Slit expression would phenocopy the islet organization defects in *Robo βKO* islets. Whole-body *Slit1*-null ($Slit1^{GFP/GFP}$) and *Slit3*-null ($Slit3^{LacZ/LacZ}$) mice are viable to adulthood. We performed positional cell counting on the islets of these mice as we have previously described (Adams et al., 2018) to determine whether these mutants exhibited islet organizational defects. In contrast to the phenotype seen in *Robo βKO* islets, individual *Slit1* or *Slit3* mutant islets have

93 completely normal architecture (Figure 3A-C). α-, β-, and δ-cells remain restricted to their respective
94 niches; the β-cells reside in the core, while the α- and δ-cells remain in the islet mantle. We also found
95 no significant difference between control islets and *Slit1* or *Slit3* mutant islets in islet size (Figure 3D) or
96 circularity (Figure 3E). Whole-body *Slit2*-null ($Slit2^{GFP/GFP}$) animals die shortly after birth. We thus
97 examined pancreata of E18.5 $Slit2^{GFP/GFP}$ embryos. Evidence of altered islet architecture in *Robo βKO*
98 mutants can be seen at E18.5; however, we did not observe overt defects in the architecture of
99 $Slit2^{GFP/GFP}$ islets at this time point (Figure 4). Taken together, these results indicate that individual Slits
100 are not required for Robo-mediated control of islet architecture.
101
102 ***Slit2 and Slit3 compensate for each other and are required for islet morphogenesis.***
103 Slit ligands are highly similar in amino acid sequence, particularly in their Robo-binding domains (Figure
104 5A). Thus, it is possible that the different Slit ligands compensate for each other during islet
105 morphogenesis. We tested the extent to which multiple Slit ligands are required for islet architecture
106 by analyzing islet formation in combinatorial Slit mutants. $Slit1^{GFP/GFP};Slit3^{LacZ/LacZ}$ double knockouts live
107 to adulthood and appear normal, with no detectable alterations in islet architecture, size, or circularity
108 (Figure 5B-F). To circumvent the neonatal lethality of $Slit2^{GFP/GFP}$ mice, we analyzed the pancreata of
109 *Slit1/2* knockouts ($Slit1^{GFP/GFP};Slit2^{GFP/GFP}$), *Slit2/3* knockouts ($Slit2^{GFP/GFP};Slit3^{LacZ/LacZ}$), and *Slit1/2/3*
110 knockouts ($Slit1^{GFP/GFP};Slit2^{GFP/GFP};Slit3^{LacZ/LacZ}$) at E18.5 and P0. *Slit1/2* knockout islets show no
111 indications of altered architecture, but *Slit2/3* and *Slit1/2/3* knockouts have disorganized islets (Figure
112 5G). To quantify this phenotype, we scored islets as either intact (insulin-positive cells surrounded by
113 glucagon-positive cells), intermediate (clusters of insulin-positive cells disrupted by glucagon-positive
114 or non-endocrine cells), or disrupted (single cells or clusters of endocrine cells that are not forming islet

structures) (Figure 5H). Double-blinded scoring of islets from the above genotypes revealed that wild-type and *Slit1/2* knockouts have few disrupted islets and similar percentages of intact and intermediate islets (WT intact: 49%, intermediate: 40%, disrupted: 11%. *Slit1/2 KO* intact: 43%, intermediate: 46%, disrupted: 11%). *Slit2/3* and *Slit1/2/3* knockouts had fewer intact islets and increased numbers of intermediate and disrupted islets (*Slit2/3* KO intact: 8%, intermediate: 53%, disrupted: 39%. *Slit1/2/3* KO intact: 8%, intermediate: 60%, disrupted: 32%). Taken together, the data suggest that *Slit1* (expressed in the islet itself) is dispensable, while *Slit2* and *Slit3* (expressed outside of the islet) compensate for each other and are required for proper islet organization.

Deletion of all three Slits selectively in the endocrine compartment does not affect islet morphogenesis.

Our data above suggests that *Slit2* and *Slit3* are involved in islet organization. However, the source of *Slit2* is unknown. While we were unable to detect the *Slit2-GFP* reporter in the pancreas, scRNA-Seq data suggests that *Slit2* is present in pancreatic tissue during developmental stages. Further, our data suggests that *Slit2* and *Slit3* compensate for each other, and that *Slit3* is expressed externally from the islet. While it is unlikely that compensatory genes are expressed in different tissues, we nevertheless set out to test whether *Slit2* may be upregulated in endocrine cells as compensation for the absence of other Slits. We generated *Ngn3-Cre;Slit1*$^{GFP/GFP}$*;Slit2*$^{flx/flx}$*;Slit3*$^{LacZ/LacZ}$ animals. These animals have whole-body knockouts of *Slit1* and *Slit3*, with a floxed *Slit2* allele. *Ngn3*, a marker of endocrine progenitors, is active in every islet endocrine cell, thus depleting *Slit2* from the endocrine compartment only. We reasoned that if *Slit2* was required in the endocrine compartment to coordinate islet morphogenesis these mice would display disrupted islet architecture. We found that *Ngn3-*

Cre;Slit1$^{GFP/GFP}$*;Slit2*$^{flx/flx}$*;Slit3*$^{LacZ/LacZ}$ mice have intact islets, indistinct from the control (Figure 6). We concluded that *Slit2* is not supplied by islet endocrine cells, and must be supplied from extra-endocrine tissue.

Slits do not affect endocrine cell migration but may affect cell adhesion

Because *Slit2/3* and *Slit1/2/3* mutant islets are disrupted and don't cluster tightly, we wondered whether this indicated a disruption in the Slit-Robo signaling pathway, and thus a failure of β-cells to migrate properly during islet morphogenesis. We performed Transwell cell migration assays using INS-1 cells. INS-1 cells seeded in the top chamber of a cell culture insert above INS-1 conditioned media showed strong migratory activity, while INS-1 cells seeded above fresh, untreated INS-1 culture media did not (Figure 7A Left, Center, B). Interestingly, INS-1 cells treated with either a non-targeting siRNA or Robo1/2 siRNA showed similar capacities for migration when seeded above conditioned media, and very little migratory activity when seeded over INS-1 media (Figure 7A,B). We repeated this experiment and seeded INS-1 cells over INS-1 media, or INS-1 media supplemented with 10μM recombinant SLIT1, SLIT2, or SLIT3 (Figure 7C). INS-1 cells did not display any changes in migratory ability at any of these conditions, suggesting that Slit and Robo interactions may not influence the migratory ability of β-cells.

In addition to directing cell migration, the Slit/Robo pathway can also modulate cell-cell adhesions. *Robo βKO* islets (*Ins2-Cre;Robo1*$^{-/-}$*;Robo2*$^{flx/flx}$) containing an *H2B-mCherry* reporter fail to maintain their structure as intact, clustered islets after isolation from the pancreas (Figure 8). While control islets (*Ins2-Cre;Robo*$^{+/+}$*;Robo2*$^{+/+}$*)* containing the same *H2B-mCherry* reporter remain tightly compacted and neatly organized after 24 hours of culture, the *Robo βKO* islets are disorganized (noted by the arrangement of mCherry), look "fluffy" around the edges, and fall apart easily. Taken together, these

159 data suggest that Slit-Robo interactions in the pancreas may not influence the migratory ability of β-
160 cells, and may be contributing to islet morphogenesis by modulating cell-cell adhesion.
161
162 **Discussion**
163 In this study, we demonstrate that Slit ligands are required for pancreatic islet architecture.
164 Simultaneous loss of all three ligands results in a disrupted, "islet explosion-like" phenotype, which is
165 also observed in *Slit2*$^{GFP/GFP}$;*Slit3*$^{LacZ/LacZ}$ knockouts. These findings lead us to conclude that all three Slit
166 ligands are indeed present in the pancreas, and that *Slit2* and *Slit3* have redundant roles in developing
167 islet architecture.
168 The exact mechanism of Slits in islet morphogenesis is unknown; however, the presence of Robo in the
169 pancreas provides some clues. Slit and Robo are ligand-receptor binding partners in the Slit-Robo
170 signaling pathway. During mammalian development, Slit and Robo occupy adjacent tissues, specifying
171 complimentary expression patterns in the developing organism (Yuan et al., 1999). While all three Slits
172 have expression patterns unique to their specific domain, they also have overlapping regions of
173 expression, suggesting some genetic redundancy. Interestingly, *Slit2* and *Slit3* share more expression
174 domains with each other than either of them do with *Slit1* (Yuan et al., 1999). We have observed a
175 similar framework in the mouse pancreas: Robo is primarily expressed in endocrine cells (Adams et al.,
176 2018), while *Slit2* and *Slit3* have overlapping expression patterns in pancreatic mesenchyme. These
177 complimentary and overlapping regions of expression are hallmarks of ligand-receptor binding
178 partners, and suggest that mesenchymal Slits interact with endocrine Robo to coordinate islet
179 architecture. We propose that Slit signals from the mesenchyme are picked up by Robo receptors on
180 the surface of developing islet endocrine cells. Loss of this signal results in a failure of islet

morphogenesis, thus the "islet explosion" phenotype described above. It is possible that Slits are not the only signal required for morphogenesis, as some of the islets in *Slit2*$^{GFP/GFP}$;*Slit3*$^{LacZ/LacZ}$ and triple knockout animals showed evidence of appropriate clustering. Future work will determine whether other ligands or even Robo-Robo interactions are involved in islet morphogenesis.

It is commonly held that islet morphogenesis is outlined by delamination of endocrine progenitors from the pancreatic duct, followed by their migration as individual cells though the mesenchyme and aggregation into islets (Pan and Wright, 2011). We provide evidence to suggest that disruption of Slit-Robo signaling influences endocrine cell-cell adhesion, not migration, during islet morphogenesis. Rather than delamination and migration as individual cells, our data is in support of the recent observation that endocrine progenitors remain physically connected throughout islet morphogenesis (Sharon et al., 2019), and suggest that disruption of this cell-cell adhesion causes the disorganized islet architecture phenotype in both *Slit2/3*-null and *Robo* β*KO* islets.

The role of *Slit1* in the islet remains elusive. The islet architecture phenotypes seen in *Slit2*$^{GFP/GFP}$;*Slit3*$^{LacZ/LacZ}$ animals are not significantly different in triple knockouts, suggesting that *Slit1* does not have any influence on islet architecture. In addition, *Slit1* expression does not overlap with *Slit2* or *Slit3*, thus it is unlikely to be redundant. However, *Slit1* has a strong presence in islet β-cells. Given that Slits have been observed to provide a protective effect on β-cells, as well as potentiate insulin secretion in β-cells (Yang et al., 2013), it seems likely that *Slit1* has a unique role in the islet. Future work elucidating the function of *Slit1* in the islet will be instructive.

We have demonstrated that *Slit2* and *Slit3* are required for proper islet cell organization in the pancreas. Taken together, our results described here in conjunction with previously published data on

202 Robo suggest that Slit-Robo signaling is required for proper islet organization and development in the

203 mouse.

Methods

Animals

All animal experiments were conducted in accordance with the University of Wisconsin-Madison IACUC guidelines under approved protocol #M005221. *Robo1*$^{-}$*;Robo2*^{flx} (Branchfield et al., 2016), *Ins2-Cre* (Postic et al., 1999), *Ngn3-Cre* (Schonhoff et al., 2004), *H2B-mCherry* (Blum et al., 2014), *Slit1*^{GFP} , *Slit2*^{GFP} (Plump et al., 2002), *Slit3*^{LacZ} (Yuan et al., 2003), *Slit2*^{flx} (Rama et al., 2015) alleles have been previously described.

Expression Analysis

tSNE plots of sc-RNA Seq obtained from the Lynn Lab's Single Cell Gene Expression Atlas (https://lynnlab.shinyapps.io/embryonic_pancreas/) (Krentz et al., 2018).

Immunostaining

Pancreata were dissected from adult (~8week old), embryonic (E18.5), or newborn (P0) mice, fixed in 4% paraformaldehyde for 1 hour at room temperature (20-30 minutes for E18.5 and P0), preserved in 30% sucrose, embedded in OCT (Leica), then sectioned onto slides. Slides were stained according to the following protocol: 1 hour block in 10% Normal Donkey Serum in PBST, 1 hour primary antibody incubation, PBST wash, 1 hour secondary antibody incubation, PBST wash, mount in Fluoromount-G (Thermo Fisher). The following primary antibodies were used: Guinea Pig anti-Insulin 1:800 (Dako), Guinea Pig anti-Insulin 1:6 (Dako 1R002), Chicken anti-GFP 1:1000 (Abcam ab13970), Rabbit anti-Glucagon 1:200 (Cell Signaling 2760), Goat anti-Somatostatin 1:50 (Santa Cruz), Rabbit anti-Somatostatin 1:800 (Phoenix G-060-03), DAPI 1:10,000 (Sigma 9542). The following secondary

antibodies were used at 1:500: Alexa 647 anti-Guinea Pig, Alexa 594 anti-Rabbit, Alexa 594 anti-Goat, Alexa 488 anti-Rabbit, Alexa 488 anti-Chicken.

For eye analysis, tissues were dissected and fixed in 4% paraformaldehyde for 2 hours at 4°C. Tissues were preserved in a series of sucrose solutions (10%, 20% sucrose) for 1.5 hours each. Tissues were further preserved in 30% sucrose overnight, embedded in OCT, then sectioned and stained as above.

For β-galactosidase staining, tissues were fixed in 4% paraformaldehyde for 1 hour at room temperature (or 20-30 minutes for E18.5 tissue). Fixed tissues were stained with X-gal solution (Roche 11828673001) for 22 hours at 37°C, then preserved, embedded, and sectioned as above. Insulin staining on these tissues was done using the Vectastain ABC HRP kit (Vector Labs PK-4007), NovaRED kit (Vector Labs SK-4800), and mounted with VectaMount (Vector Labs H-5000). Slides for expression analysis imaged using a Zeiss Axio Observer Z1.

Cell Counting, Shape, Size Analysis

Slides used for cell counting or shape and size analysis were imaged on a Nikon A1RS confocal microscope. Confocal z-stacks were converted to maximum intensity projected images. The number of α- and δ- cells were counted using the ImageJ Cell Counter tool. α- or δ- cells were considered in the islet periphery if they were within the first two cell layers of the islet. For shape and size analysis, islets were outlined and a threshold was applied in ImageJ. The Analyze Particles tool then gave readout of islet size in microns^2 and a circularity score (between 0-1, where 1 indicates a perfect circle). A minimum of 10 islets were analyzed across at least three different tissue sections per mouse. Analysis performed on *n=3* mice for each genotype. α- and δ-cell percentages, islet size, and islet circularity values were averaged for each mouse and plotted in Prism.

248

249 Amino Acid Alignment

250 Amino acid sequence and domain information were obtained from Yuan et al., 1999. Pairwise
251 alignment scores of amino acid sequences were provided by ClustalW (https://www.genome.jp/tools-
252 bin/clustalw).

253

254 Islet Scoring

255 Islet scoring was performed on images of tissue sections stained for insulin, glucagon, and DAPI. Z-stack
256 images were converted to maximum intensity projected images, and randomly assigned a number
257 identifier. Four independent trials (by four different researchers) of double-blinded scoring was
258 performed on 197 images, comprising at least 10 images spanning four different tissue sections per
259 mouse, and at least 3 mice per genotype.

260

261 siRNA Treatment and Transwell Cell Migration Assay

262 INS-1 cells (AddexBio) were maintained in culture media containing RPMI-1640 (ThermoFisher), 10%
263 FBS, 1% penicillin/streptomycin, and supplemented with 0.05mM β-mercaptoethanol. For siRNA
264 treatment, cells were treated with either 60nM ON-TARGETplus Non-targeting siRNA or 30nM each
265 *Robo1* and *Robo2* ON-TARGETplus SMARTPool siRNA (Horizon Discovery). siRNA knockdown was
266 confirmed by qPCR using Brilliant III Ultra-Fast SYBR Green reagents, Robo primers (*Robo1*: 5'-
267 AACTGCTGCACAGCCAGCAA-3', 5'-TGCTATACAATCAGCTGGGCGAC-3', *Robo2*: 5'-
268 ACCAGGGGTTGGATCAGAGGAG-3', 5'-TCTCAGCCTTCCGAGGACCA-3'), and *β-actin* primers (5'-
269 TGCTCAGCCTGTACGCAACA-3', 5'-CCCGCAATGTCTACCCGCAT-3'), run on a CFX Connect Instrument

(Bio-Rad). After siRNA treatment, cells were seeded at a density of 250,000 cells/mL in Transwell cell culture inserts with 8μM pores (Sigma). Inserts were placed into wells containing either 700μL INS-1 culture media or 700μL INS-1 conditioned media and cultured at 37°C for 48 hours. Inserts were then fixed in 4% paraformaldehyde for 20 minutes, unmigrated cells were wiped off the top of the insert, and then inserts were incubated in 0.08% crystal violet and a 1:10,000 concentration of DAPI to visualize the cells. Nine non-overlapping field of view images were taken for each insert. Three images per insert were chosen at random for quantification. Results are reported as the average number of cells that migrated per field of view. Recombinant SLIT cell migration experiments were performed as described with INS-1 cells seeded in Transwell inserts placed in wells containing INS-1 media, INS-1 conditioned media, or INS-1 media supplemented with 10μM Recombinant SLIT1, SLIT2, or SLIT3 (R&D Systems).

Islet Isolation

Mice were perfused through the bile duct with 0.8mM Collagenase P (Roche) in 1xDMEM (ThermoFisher). Pancreata were removed and digested by reciprocal shaking in a 37°C water bath at 200 RPM. Islets were purified by gradient centrifugation in Histopaque-1077 and -1119 (Sigma), cultured overnight at 37°C in 1xDMEM, 10% FBS, and 1% penicillin/streptomycin, and imaged the following day.

Statistical Analysis

All data reported as mean ±SEM unless otherwise indicated. P-values calculated using Student's T-test in Prism GraphPad 7 unless otherwise indicated. Any p-value <0.05 was considered significant and marked with an asterisk.

Author Contributions

Conceptualization, B.B. and J.M.G; Methodology, B.B. and J.M.G; Investigation, J.M.G, M.T.A., N.S, and H.J.; Formal Analysis, J.M.G, M.T.A., N.S, and H.J.; Writing Original Draft, B.B and J.M.G.; Writing, Review and Editing, all authors; Funding Acquisition, B.B.; Supervision, B.B.

Acknowledgements

We thank members of the Blum lab, especially Bayley Waters and Dex Nimkulrat for valuable discussion and comments on the manuscript. We thank Le Ma, David Ornitz, Alain Chedotal, and Marc Tessier-Lavigne for mice. We are grateful to Francis Lynn and Nicole Krentz for allowing us to use their scRNA-seq data, and to Cody Frederickson for help generating figures. We are also grateful to Lance Rodenkirch and the UW-Madison Optical Imaging Core for help with imaging. This work was funded in part by the following grants. R01DK121706 from the NIDDK, the DRC at Washington University Pilot Grant P30DK020579, and Pilot Award UL1TR000427 from the UW-Madison Institute for Clinical and Translational Research (ICTR). JMG and MTA were funded by 5T32GM007133-44, a graduate training award from the UW-Madison Stem Cell & Regenerative Medicine Center, and an Advanced Opportunity Fellowship through SciMed Graduate Research Scholars at UW-Madison.

References

Adams, M. T., Gilbert, J. M., Hinojosa Paiz, J., Bowman, F. M. and Blum, B. (2018). Endocrine cell type sorting and mature architecture in the islets of Langerhans require expression of Roundabout receptors in β cells. *Sci. Rep.* **8**, 10876.

Baetens, D., Stefan, Y., Ravazzola, M., Malaisse-Lagae, F., Coleman, D. L. and Orci, L. (1978). Alteration of islet cell populations in spontaneously diabetic mice. *Diabetes* **27**, 1–7.

Blockus, H. and Chédotal, A. (2016). Slit-Robo signaling. *Development* **143**, 3037–3044.

Blum, B., Roose, A. N., Barrandon, O., Maehr, R., Arvanites, A. C., Davidow, L. S., Davis, J. C., Peterson, Q. P., Rubin, L. L. and Melton, D. A. (2014). Reversal of β cell de-differentiation by a small molecule inhibitor of the TGFβ pathway. *Elife* **3**, e02809.

Branchfield, K., Nantie, L., Verheyden, J. M., Sui, P., Wienhold, M. D. and Sun, X. (2016). Pulmonary neuroendocrine cells function as airway sensors to control lung immune response. *Science (80-.).* **351**, 707–710.

Brose, K., Bland, K. S., Wang, K. H., Arnott, D., Henzel, W., Goodman, C. S., Tessier-lavigne, M., Kidd, T., Way, D. N. A. and Francisco, S. S. (1999). Slit Proteins Bind Robo Receptors and Have an Evolutionarily Conserved Role in Repulsive Axon Guidance. **96**, 795–806.

Cabrera, O., Berman, D. M., Kenyon, N. S., Ricordi, C., Berggren, P.-O. and Caicedo, A. (2006). The unique cytoarchitecture of human pancreatic islets has implications for islet cell function. *Proc. Natl. Acad. Sci. U. S. A.* **103**, 2334–9.

Chédotal, A. (2007). Slits and their receptors. *Adv. Exp. Med. Biol.* **621**, 65–80.

Delloye-Bourgeois, C., Jacquier, A., Charoy, C., Reynaud, F., Nawabi, H., Thoinet, K., Kindbeiter, K., Yoshida, Y., Zagar, Y., Kong, Y., et al. (2015). PlexinA1 is a new Slit receptor and mediates axon

guidance function of Slit C-terminal fragments. *Nat. Neurosci.* **18**, 36–45.

Dickson, B. J. and Gilestro, G. F. (2006). Regulation of Commissural Axon Pathfinding by Slit and its Robo Receptors. *Annu. Rev. Cell Dev. Biol.* **22**, 651–675.

Escot, S., Willnow, D., Naumann, H., Di Francescantonio, S. and Spagnoli, F. M. (2018). Robo signalling controls pancreatic progenitor identity by regulating Tead transcription factors. *Nat. Commun.* **9**, 5082.

Hivert, B. (2002). Robo1 and Robo2 Are Homophilic Binding Molecules That Promote Axonal Growth. *Mol. Cell. Neurosci.* **21**, 534–545.

Kilimnik, G., Zhao, B., Jo, J., Periwal, V., Witkowski, P. and Misawa, R. (2011). Altered Islet Composition and Disproportionate Loss of Large Islets in Patients with Type 2 Diabetes. **6**,.

Kim, A., Miller, K., Jo, J., Kilimnik, G., Wojcik, P. and Hara, M. (2009). Islet architecture: A comparative study. *Islets* **1**, 129–136.

Krentz, N. A., Lee, M., Xu, E. E., Sasaki, S. and Lynn, F. C. (2018). Single cell transcriptome profiling of mouse and hESC-derived pancreatic progenitors. *bioRxiv* 289470.

Pan, F. C. and Wright, C. (2011). Pancreas organogenesis: From bud to plexus to gland. *Dev. Dyn.* **240**, 530–565.

Plump, A. S., Erskine, L., Sabatier, C., Brose, K., Epstein, C. J., Goodman, C. S., Mason, C. A. and Tessier-Lavigne, M. (2002). Slit1 and Slit2 cooperate to prevent premature midline crossing of retinal axons in the mouse visual system. *Neuron* **33**, 219–232.

Postic, C., Shiota, M., Niswender, K. D., Jetton, T. L., Chen, Y., Moates, J. M., Shelton, K. D., Lindner, J., Cherrington, A. D. and Magnuson, M. A. (1999). Dual roles for glucokinase in glucose homeostasis as determined by liver and pancreatic β cell-specific gene knock-outs using Cre

recombinase. *J. Biol. Chem.* **274**, 305–315.

Rama, N., Dubrac, A., Mathivet, T., Ní Chárthaigh, R.-A., Genet, G., Cristofaro, B., Pibouin-Fragner, L., Ma, L., Eichmann, A. and Chédotal, A. (2015). Slit2 signaling through Robo1 and Robo2 is required for retinal neovascularization. *Nat. Med.* **21**, 483–491.

Roscioni, S. S., Migliorini, A., Gegg, M. and Lickert, H. (2016). Impact of islet architecture on β-cell heterogeneity, plasticity and function. *Nat. Rev. Endocrinol.* **12**, 695–709.

Schonhoff, S. E., Giel-Moloney, M. and Leiter, A. B. (2004). Neurogenin 3-expressing progenitor cells in the gastrointestinal tract differentiate into both endocrine and non-endocrine cell types. *Dev. Biol.* **270**, 443–454.

Sharon, N., Chawla, R., Mueller, J., Gifford, D. K., Trapnell, C., Melton, D., Sharon, N., Chawla, R., Mueller, J., Vanderhooft, J., et al. (2019). Differentiation with Morphogenesis to Generate A Peninsular Structure Coordinates Asynchronous Differentiation with Morphogenesis to Generate Pancreatic Islets. 1–15.

Steiner, D. J., Kim, A., Miller, K. and Hara, M. (2010). Pancreatic islet plasticity: Interspecies comparison of islet architecture and composition. *Islets* **2**,.

Svensson, K. J., Long, J. Z., Jedrychowski, M. P., Cohen, P., Lo, J. C., Serag, S., Kir, S., Shinoda, K., Tartaglia, J. A., Rao, R. R., et al. (2016). A secreted slit2 fragment regulates adipose tissue thermogenesis and metabolic function. *Cell Metab.* **23**, 454–466.

Tong, M., Jun, T., Nie, Y., Hao, J. and Fan, D. (2019). The role of the SLIT/Robo signaling pathway. *J. Cancer* **10**, 2694–2705.

Wright, K. M., Lyon, K. A., Leung, H., Leahy, D. J., Ma, L. and Ginty, D. D. (2012). Dystroglycan Organizes Axon Guidance Cue Localization and Axonal Pathfinding. *Neuron* **76**, 931–944.

Wu, M. F., Liao, C. Y., Wang, L. Y. and Chang, J. T. (2017). The role of Slit-Robo signaling in the regulation of tissue barriers. *Tissue Barriers* **5**, 1–17.

Yang, Y. H. C., Manning Fox, J. E., Zhang, K. L., MacDonald, P. E. and Johnson, J. D. (2013). Intraislet SLIT-ROBO signaling is required for beta-cell survival and potentiates insulin secretion. *Proc. Natl. Acad. Sci. U. S. A.* **110**, 16480–5.

Ypsilanti, A. R. and Chedotal, A. (2014). Roundabout receptors. *Adv. Neurobiol.* **8**, 133–64.

Ypsilanti, A. R., Zagar, Y. and Chedotal, A. (2010). Moving away from the midline: new developments for Slit and Robo. *Development* **137**, 1939–1952.

Yuan, W., Zhou, L., Chen, J. H., Wu, J. Y., Rao, Y. and Ornitz, D. M. (1999). The mouse SLIT family: secreted ligands for ROBO expressed in patterns that suggest a role in morphogenesis and axon guidance. *Dev. Biol.* **212**, 290–306.

Yuan, W., Rao, Y., Babiuk, R. P., Greer, J. J., Wu, J. Y. and Ornitz, D. M. (2003). A genetic model for a central (septum transversum) congenital diaphragmatic hernia in mice lacking Slit3. *Proc Natl Acad Sci USA* **100**, 5217–5222.

Zhang, B., Dietrich, U. M., Geng, J. G., Bicknell, R., Esko, J. D. and Wang, L. (2009). Repulsive axon guidance molecule Slit3 is a novel angiogenic factor. *Blood* **114**, 4300–4309.

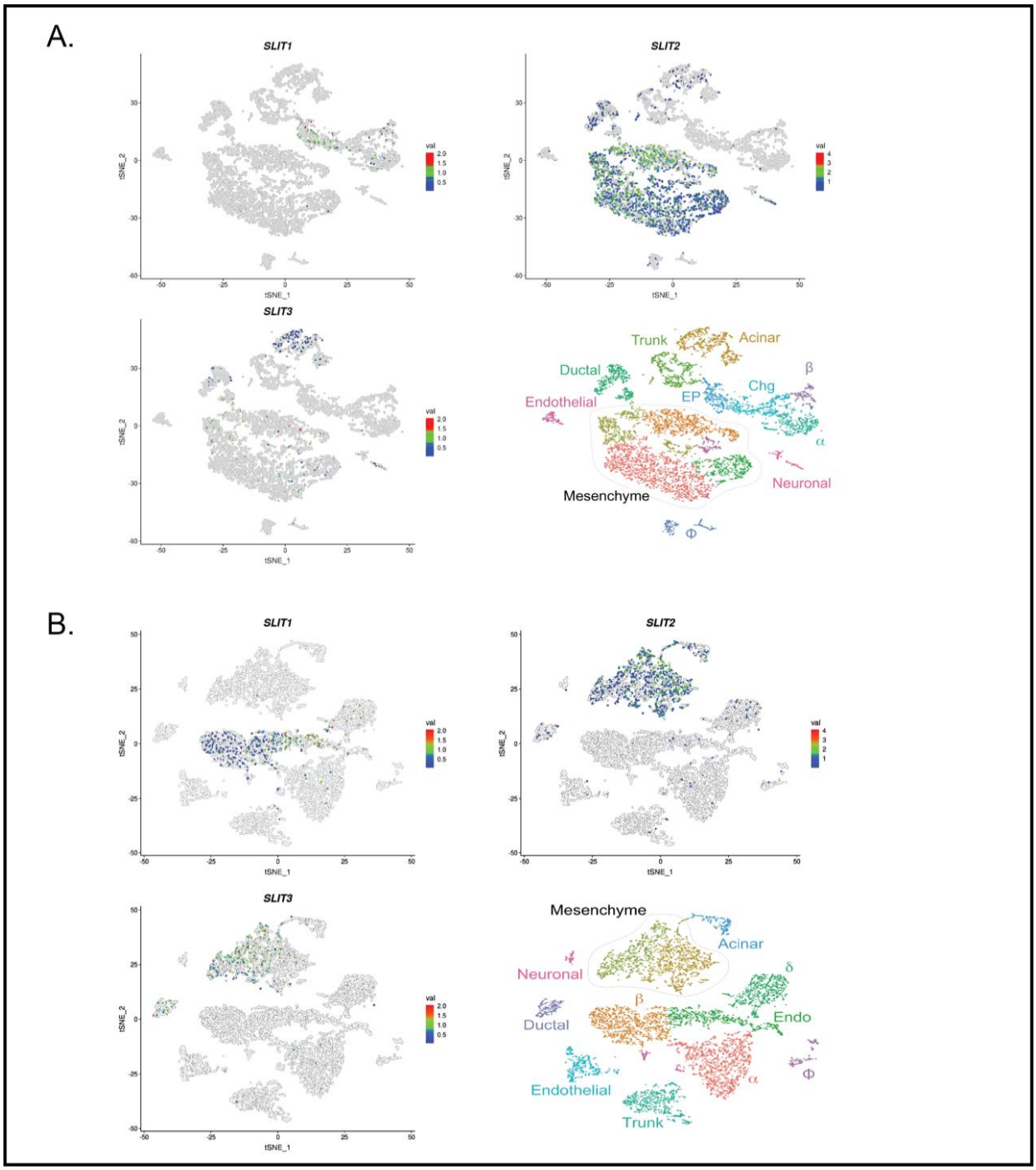

Figure 1: Slit transcripts are expressed in different compartments in the developing murine pancreas. *Single-cell RNA-Seq data (scRNA-Seq) adapted from Krentz and colleagues (Krentz et al. 2018). tSNE plots depicting Slit1, Slit2, and Slit3 expression in pancreatic cells. Time points analyzed are E15.5 (A) and E18.5 (B). Slit1 is restricted to the endocrine compartment, while Slit2 and Slit3 localize with the mesenchyme/acinar compartment.*

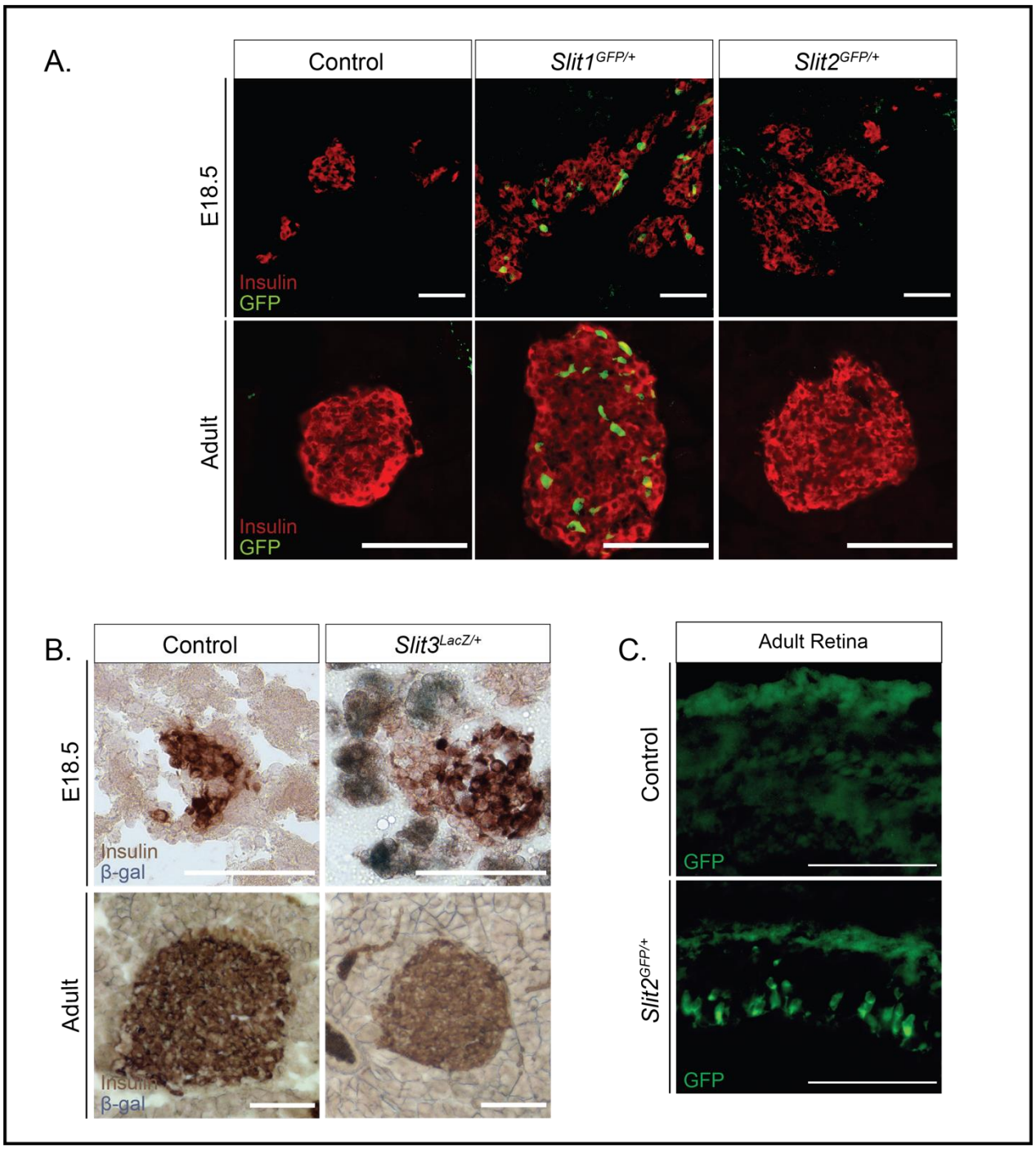

Figure 2: Slit1, but not Slit2 or Slit3, is expressed in the mouse pancreas from embryonic stages to adulthood. *(A) Immunofluorescence staining of β-cells (Insulin, red) and Slit1, Slit2 (GFP, green) in E18.5 and adult heterozygous knock-in mice. (B) β-gal staining of Slit3 (LacZ, blue) in E18.5 and adult heterozygous knock-in mice. β-gal staining (Slit3 expression) is apparent in non-endocrine tissue surrounding the islet in the embryo. (C) Immunofluorescence staining of Slit2 (GFP, green) in retinal sections from control (wild type) or Slit2$^{GFP/+}$ heterozygous animals. Scale bar = 100 microns.*

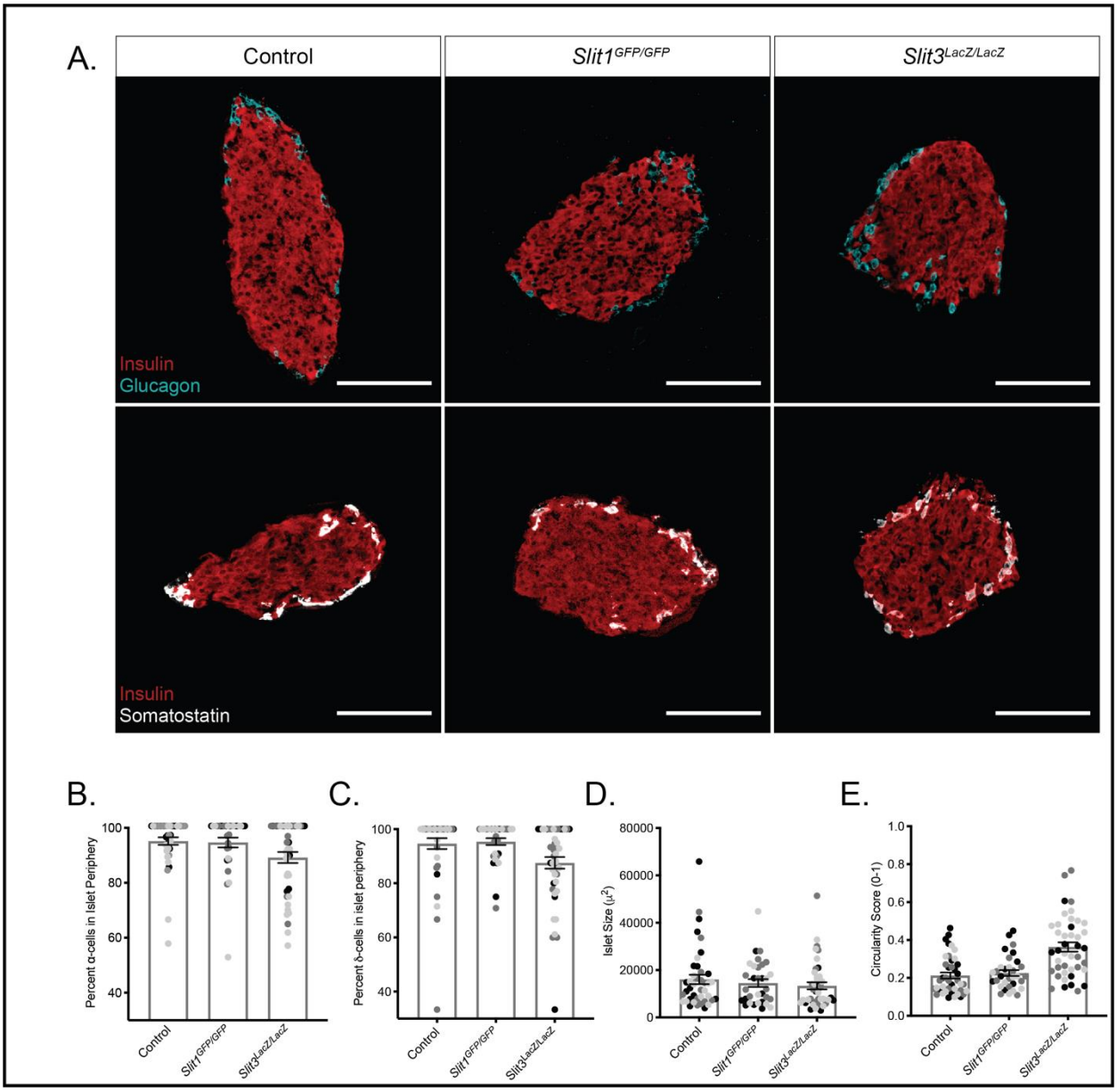

Figure 3: Loss of a single Slit ligand does not compromise islet architecture. *(A) Immunofluorescence staining of β-cells (Insulin, red), α-cells (Glucagon, cyan) and δ-cells (Somatostatin, white) in adult (~8 week old) homozygous knockout mice. Scale bar = 100 microns. (B) Percentage of α-cells found in the islet periphery out of total α-cells. (C) Percentage of δ-cells found in the islet periphery out of total δ-cells. (D) Average islet size (E) Average islet circularity (as noted by a circularity score of 0-1, where 1 is a perfect circle). Data presented as mean ±SEM.*

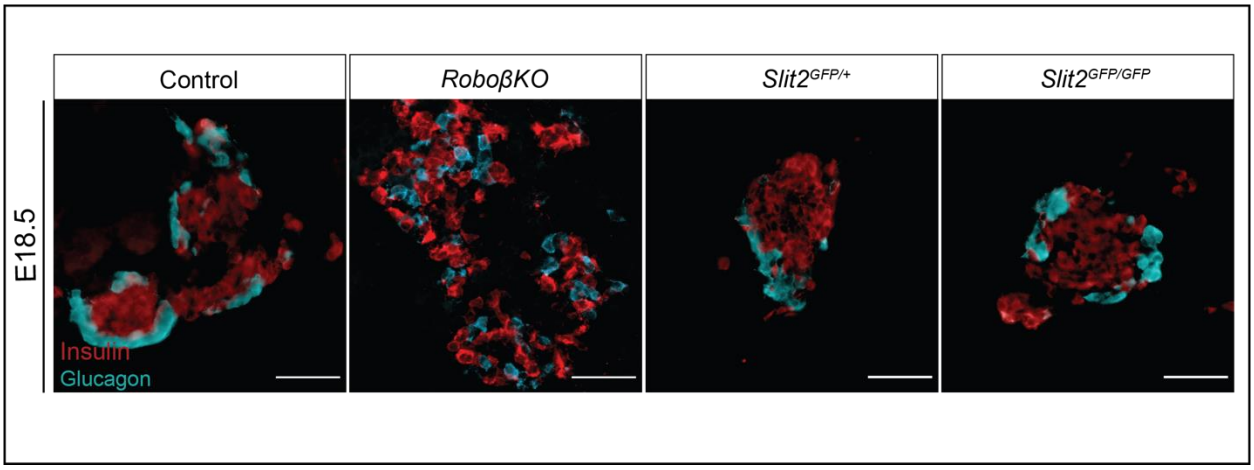

Figure 4: Slit2 knockout embryos do not have islet architectural defects. *Immunofluorescence staining of β-cells (Insulin, red) and α-cells (Glucagon, cyan) in E18.5 control, Ins2-Cre;Robo1$^{-/-}$;Robo2$^{flx/flx}$, and Slit2 mice. Scale bar = 50 microns.*

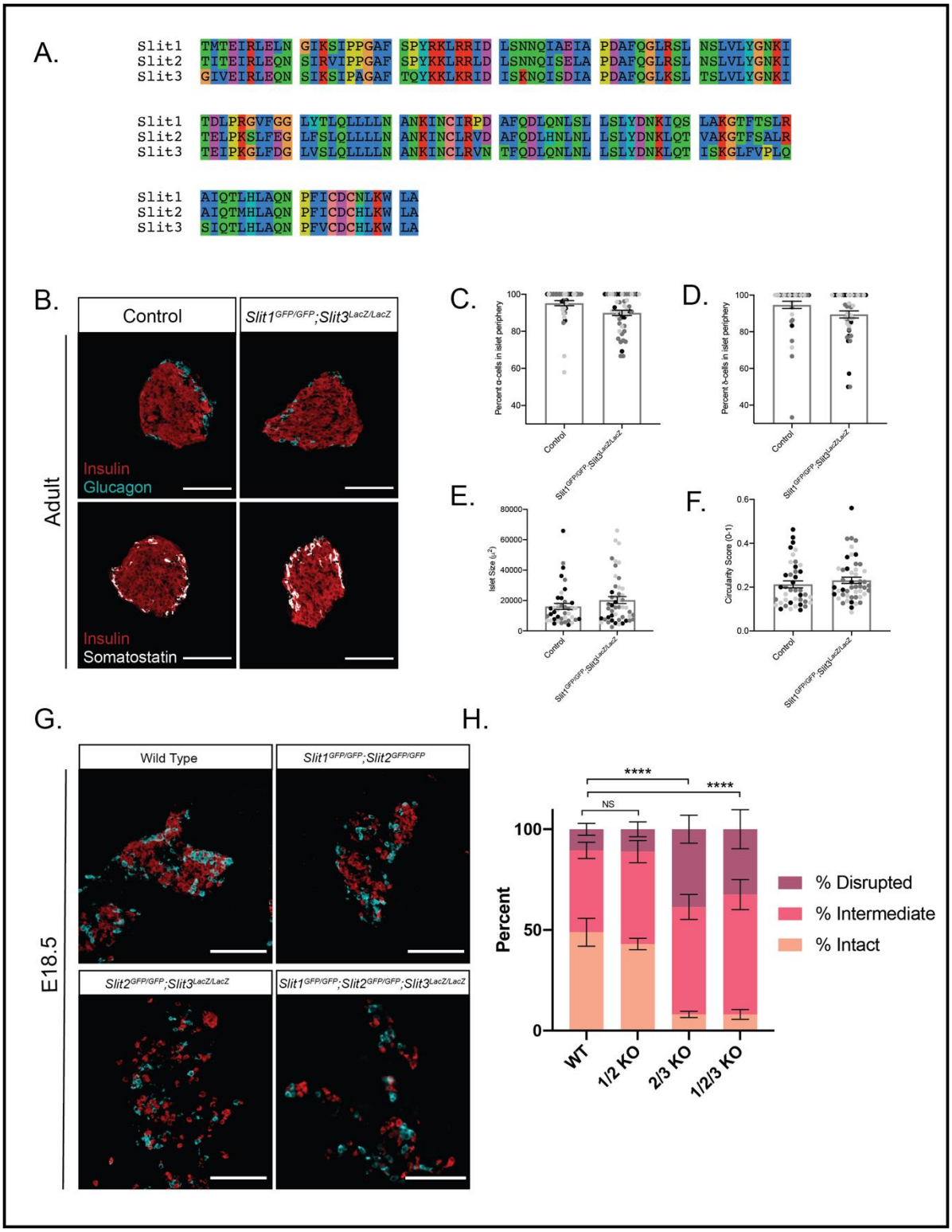

Figure 5: Slit2 and Slit3 compensate for one another in islet morphogenesis. *(A) Amino acid alignment of the Robo-binding domain LRR2 (Slit1: 310aa-451aa, Slit2: 301aa-442aa, Slit3: 308aa-449aa) of all three murine Slits. In this region, the pairwise alignment scores are: Slit1/Slit2: 77%, Slit1/Slit3: 69%, Slit2/Slit3: 70%. (B) Immunofluorescence staining of β-cells*

(Insulin, red), α-cells (Glucagon, cyan) and δ-cells (Somatostatin, white) in adult (~8 week old) homozygous Slit1$^{GFP/GFP}$;Slit3$^{LacZ/LacZ}$ knockout mice. Scale bar = 100 microns. (C) Percentage of α-cells found in the islet periphery out of total α-cells. (D) Percentage of δ-cells found in the islet periphery out of total δ-cells. (E) Average islet size (F) Average islet circularity (as noted by a circularity score of 0-1, where 1 is a perfect circle). Data presented as mean ±SEM. (G) Immunofluorescence staining of β-cells (Insulin, red) and α-cells (Glucagon, cyan) in control (wild-type), double, and triple knockout mice at E18.5/P0. Scale bar = 100 microns. (H) Percentage of islets from each genotype that were scored as intact, intermediate, or disrupted. Data presented as mean ±SEM. p <0.0001; Chi-square test.

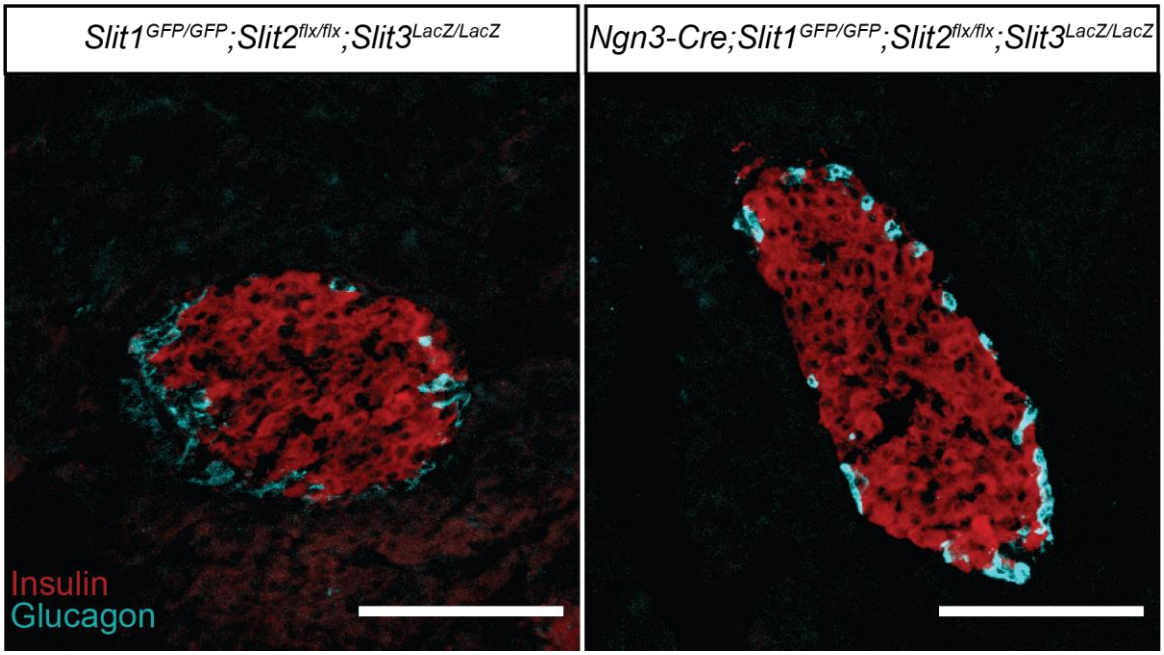

Figure 6: Deletion of all three Slits in the endocrine compartment does not affect islet morphogenesis. *Immunofluorescence staining of β-cells (Insulin, red) and α-cells (Glucagon, cyan) in adult (~8 week old) Slit1$^{GFP/GFP}$;Slit2$^{flx/flx}$;Slit3$^{LacZ/LacZ}$ mice with and without Ngn3-Cre. Scale bar = 100 microns.*

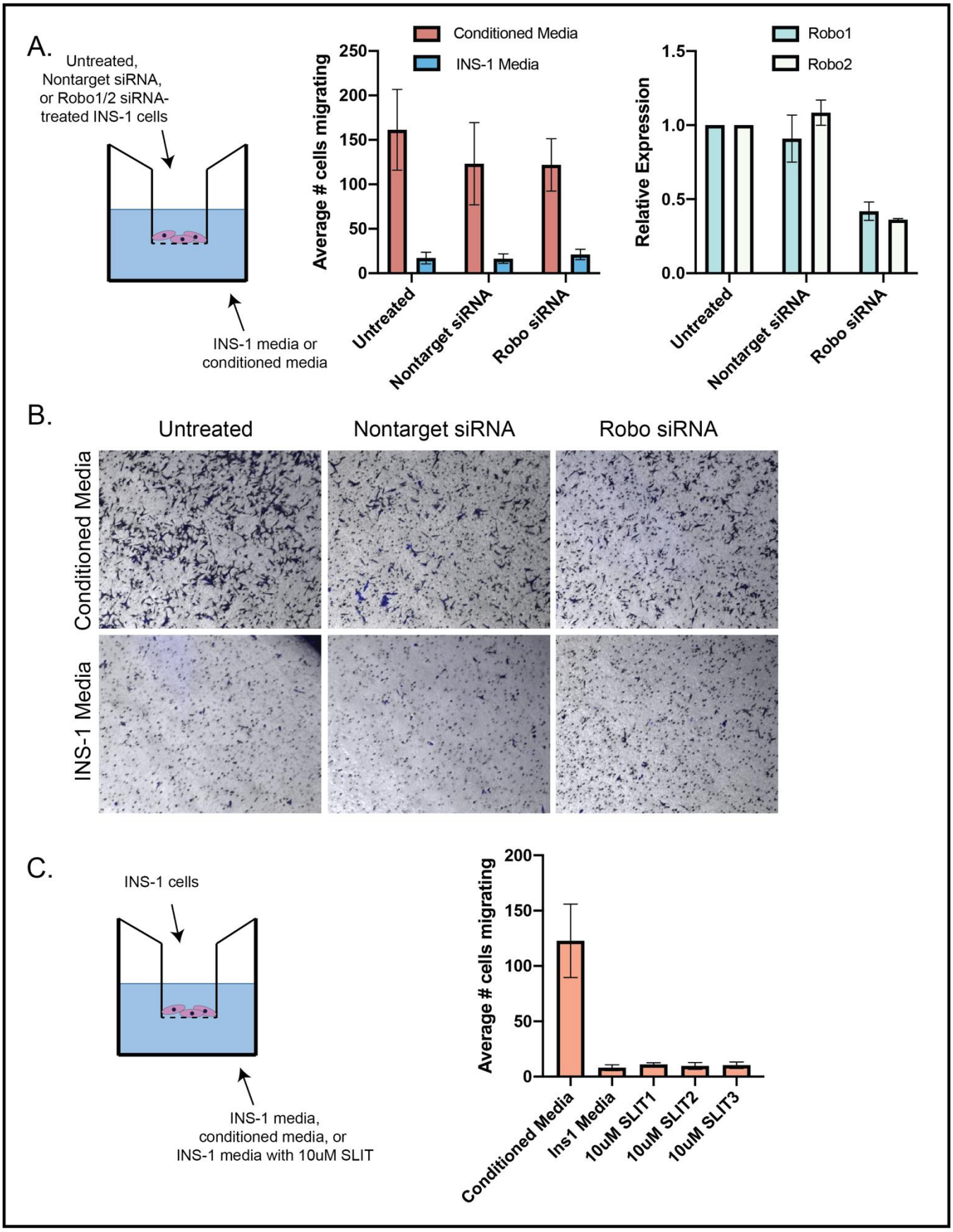

Figure 7: Islet architecture changes are likely not due to changes in migratory ability. *(A) (Left) Transwell cell migration assay. INS-1 cells either untreated, treated with a nontarget siRNA, or treated with Robo1/2 siRNA were seeded in cell culture inserts over INS-1 conditioned media, or fresh INS-1 culture media. Data presented as mean ±SEM. (Center) Results of cell migration assay. The average number of cells migrating per field of view (see B) is plotted. Data presented as mean ±SEM (Right) qPCR validation of siRNA-mediated knockdown of Robo1 and Robo2. (B) Representative images of a single field of view of a cell migration insert used in the experiments shown in (A). (C) (Left) Transwell cell migration assay. INS-1 cells were seeded in cell culture inserts over INS-1 conditioned media, fresh INS-1 culture media, or fresh INS-1 culture media supplemented with 10μM recombinant SLIT. The average number of cells migrating per field of view is plotted. Data presented as mean ±SEM.*

Figure 8: Robo βKO islets have cell-cell adhesion defects. *Representative images of isolated islets from control (Ins2-Cre;Robo1$^{+/+}$;Robo2$^{+/+}$) or RoboβKO (Ins2-Cre;Robo1$^{-/-}$;Robo2$^{flx/flx}$) animals containing an H2B-mCherry reporter after 24 hours in culture. mCherry marks Cre-mediated recombination in β-cell nuclei. Robo βKO islets look "fluffy" and fall apart after isolation.*